

Blindsight depends on the lateral geniculate nucleus

Michael C. Schmid¹, Sylwia W. Mrowka¹, Janita Turchi¹, Richard C. Saunders¹, Melanie Wilke¹, Andrew J. Peters¹, Frank Q. Ye² & David A. Leopold^{1,2}

Injury to the primary visual cortex (V1) leads to the loss of visual experience. Nonetheless, careful testing shows that certain visually guided behaviours can persist even in the absence of visual awareness^{1–4}. The neural circuits supporting this phenomenon, which is often termed blindsight, remain uncertain⁴. Here we demonstrate that the thalamic lateral geniculate nucleus (LGN) has a causal role in V1-independent processing of visual information. By comparing functional magnetic resonance imaging (fMRI) and behavioural measures with and without temporary LGN inactivation, we assessed the contribution of the LGN to visual functions of macaque monkeys (*Macaca mulatta*) with chronic V1 lesions. Before LGN inactivation, high-contrast stimuli presented to the lesion-affected visual field (scotoma) produced significant V1-independent fMRI activation in the extrastriate cortical areas V2, V3, V4, V5/middle temporal (MT), fundus of the superior temporal sulcus (FST) and lateral intraparietal area (LIP) and the animals correctly located the stimuli in a detection task. However, following reversible inactivation of the LGN in the V1-lesioned hemisphere, fMRI responses and behavioural detection were abolished. These results demonstrate that direct LGN projections to the extrastriate cortex have a critical functional contribution to blindsight. They suggest a viable pathway to mediate fast detection during normal vision.

We acclimated two adult macaque monkeys with chronic V1 aspiration-lesions (Methods Summary) to the fMRI-testing environment. During the experiments, the animals sat upright in a custom-made

chair placed in a vertical 4.7 T magnetic resonance scanner, and fixated on a small point in the centre of the screen while we recorded the eye position and presented visual stimuli (Supplementary Methods). We established the boundaries of the retinotopically organized visual areas using standard functional mapping methods⁵ (Supplementary Figs 1, 2). The centre of the lesion was located at the representation of the horizontal meridian, and extended several millimetres both dorsally and ventrally into V1 (black area in Fig. 1a, area between red bars in Fig. 1b, black area in Supplementary Fig. 2), corresponding to a visual eccentricity of $\sim 2^\circ$ to $\sim 7^\circ$ of visual angle. Previous work has shown that this type of lesion in V1 does not alter the retinotopic organization assessed with fMRI in several extrastriate areas⁶.

To assess whether the extrastriate cortex could be activated in the absence of V1 input, we presented a small (2° diameter) rotating chequerboard pattern, known to effectively drive responses in the early visual cortex, to the visual field region affected by the lesion (scotoma, Fig. 1c, top). In independent experimental runs, we presented the stimulus to the corresponding region in the healthy hemisphere as a control (Fig. 1c, bottom). As expected, the stimulus shown to the unaffected hemifield elicited strong, circumscribed, contralateral responses in V1, neighbouring extrastriate areas V2, V3, V4, V5/MT and FST (Fig. 2a, d), and parietal area LIP (Supplementary Fig. 3a, c). When the stimulus was presented inside the scotoma region, there was no V1 response because the cortex had been removed; nonetheless, there were stimulus-driven responses in

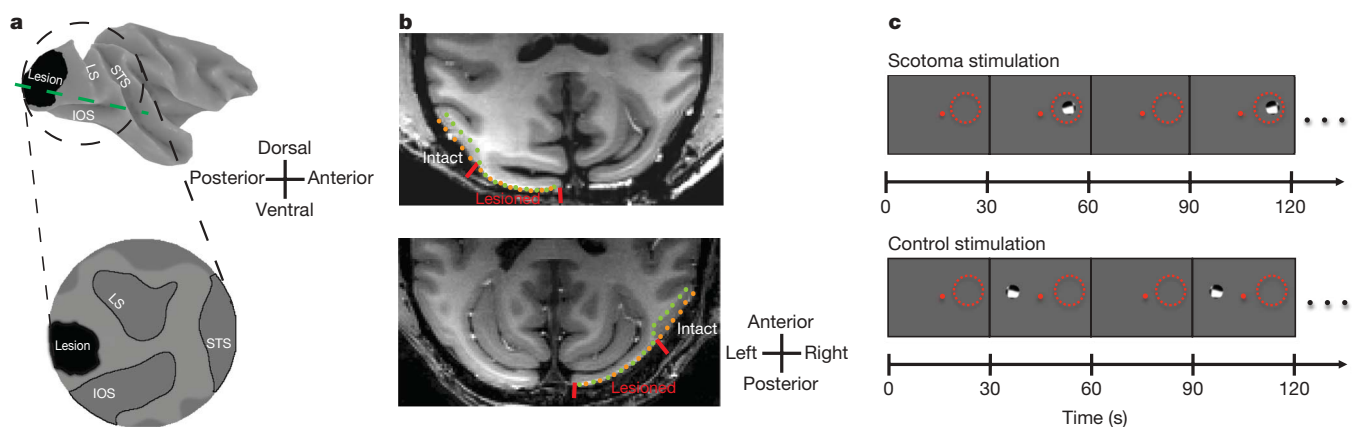


Figure 1 | Experimental set-up. **a**, A side view on the right hemisphere of an inflated macaque brain. An area of $\sim 400 \text{ mm}^2$ of grey matter in the opercular part of V1, representing the visual field between $\sim 2^\circ$ and 7° , has been surgically aspirated and is shown in black. Extrastriate areas, the subject of analysis in this study, are hidden in the sulci surrounding V1, including the lunate (LS), inferior occipital (IOS) and superior temporal (STS) sulci. To facilitate the visual examination of extrastriate cortex, the occipital lobe (dashed circled area) was cut and flattened (inset). **b**, Axial sections of monkey 1's (top) and monkey 2's (bottom) occipital lobes at the

position indicated by the green dashed line in **a**. The outward borders of white and grey matter are highlighted by green and orange dotted lines, respectively. The lesions are evident by the absence of grey matter (area between red line markers). **c**, To compare visually elicited responses in the extrastriate cortex in the presence of V1 input to those in its absence, we spatially restricted (2° diameter) rotating chequerboard stimuli and presented them either inside (top) or outside (bottom) the scotoma (part of the visual field affected by the V1 lesion, indicated here by red dotted circles; the single red dot indicates the fixation point for the animal).

¹Laboratory of Neuropsychology, National Institute of Mental Health (NIMH), 49 Convent Drive, Bethesda, Maryland 20892, USA. ²Neurophysiology Imaging Facility, NIMH, National Institute of Neurological Disorders and Stroke (NINDS), National Eye Institute (NEI), 49 Convent Drive, Bethesda, Maryland 20892, USA.

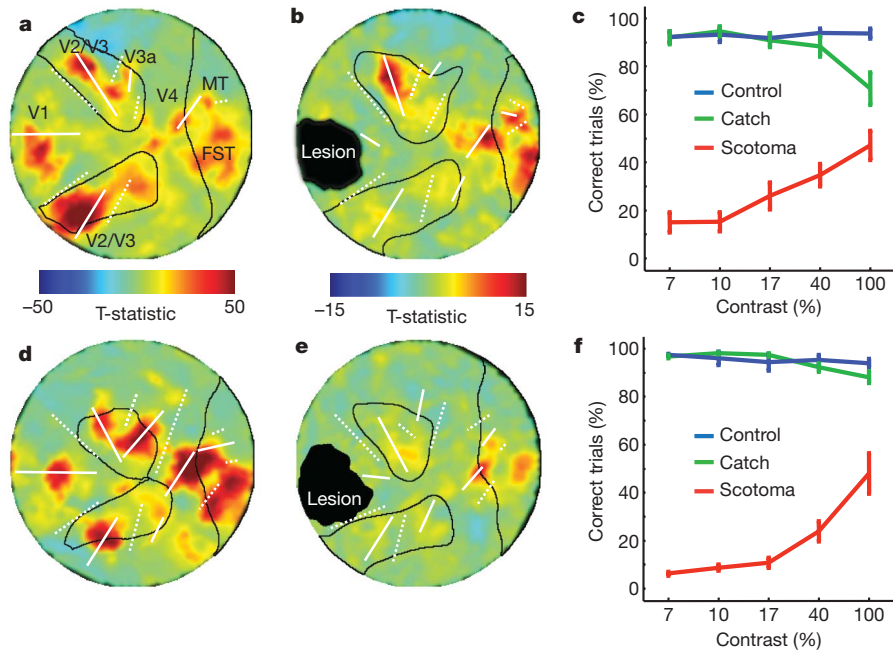


Figure 2 | Visual processing in V1-lesioned monkeys. **a**, Functional activation map (t -statistic) of monkey 1's non-lesioned visual cortex to 85 cycles of visual stimulation outside the scotoma (see Fig. 1c, bottom). The map has been horizontally flipped for easier comparison with the lesioned hemisphere. White dotted and solid lines show the position of the vertical and horizontal meridian representations, respectively, derived from independent retinotopic mapping experiments (Supplementary Figs 1, 2) to reveal the functional boundaries of extrastriate areas^{5,6}. **b**, Activation map of monkey 1's lesioned hemisphere to 85 cycles of visual stimulation inside the scotoma (see Fig. 1c, bottom). The position of the stimulus inside the scotoma was effective in that the lesion surrounding the V1 cortex with intact grey matter was not activated. In the absence of V1 input, areas V2, V3, V4 and V5/MT continue to be visually responsive. **c**, Behavioural performance of monkey 1 in detecting visual stimuli (0.2° diameter)

extrastriate areas V2, V3, V4, V5/MT, FST and LIP (Fig. 2b, e and Supplementary Fig. 3b, d), indicating that stimulus information reached these areas in the absence of V1 input. Moreover, comparing the activation patterns of the lesioned and control hemispheres revealed that the responses within each area were localized to their normal retinotopic positions. One prominent difference between the lesioned and control conditions was the emergence of dorsoventral asymmetry in areas V2 and V3, with only dorsal, but not ventral, portions of these areas exhibiting V1-independent responses. This effect, which has also been observed in human blindsight⁷, cannot be attributed to the position of either the lesion or the stimulus, as the retinotopically matched stimulus in the opposite visual field evoked roughly equivalent responses in the dorsal and ventral parts.

On the behavioural level, both monkeys retained the ability to detect and make a saccadic eye movement to small (0.2° diameter) high-contrast, but not low-contrast, visual targets presented inside the scotoma, albeit with diminished performance. Target contrasts were adjusted based on performance in the control hemifield, such that there was reliable detection even at the lowest contrast level (7%) (Fig. 2c, f and Supplementary Methods). When low-contrast stimuli were presented inside the scotoma, both monkeys consistently maintained central fixation, indicating that they were unaware that any stimulus was being presented². By comparison, when we showed high-contrast (100%) stimuli, the monkeys were able to detect roughly half of the presentations, consistent with previous reports of blindsight in humans and monkeys^{1-4,8}. Finally, a direct comparison between detection performance and fMRI responses to the same set of stimuli (2° diameter) presented in the scotoma at varying luminance contrast levels confirmed the tight relationship between the two measures of blindsight (Supplementary Fig. 4).

presented inside (red line) or outside (green line) the scotoma at different luminance contrast levels compared to a constant grey background. On one third of the trials, no stimulus was presented and the monkey was rewarded for maintaining central fixation (blue line). Data represent mean \pm s.e.m. from five experiments. **d**, Functional activation map of monkey 2's non-lesioned hemisphere to 95 cycles of visual stimulation outside the scotoma. **e**, Activation map of monkey 2's lesioned hemisphere to 95 cycles of visual stimulation inside the scotoma. **f**, Behavioural performance of monkey 2 for detecting visual stimuli inside (red line) and outside (blue line) the scotoma or during catch trials (green line). Data represent mean \pm s.e.m. from five experiments. Although both monkeys display a large visual deficit, they continue to process visual information to some extent as performance improves with stimulus contrast.

Several controls ruled out the possibility that scattered light was contributing to the observed behavioural and fMRI responses to stimuli in the scotoma effects^{9,10}: first, behavioural responses were spatially accurate, as performance was calculated by considering only saccades that were within 1° of the target. Second, when the same high-contrast stimuli were presented monocularly in the monkeys' blindspots (the area covered by the optic disk in the retina), their performance fell to zero (Supplementary Fig. 5). Third, no systematic fMRI modulation was measured in the intact V1 of either monkey adjacent to the lesion (Fig. 2b, e). Fourth, strong extrastriate activation was found in a third monkey, in which we made a much larger lesion, encompassing opercular V1 and a portion of the adjacent V2 (Supplementary Fig. 6). As well as ruling out non-specific effects of scattering light^{9,10} as responsible for the observed effects, these experiments demonstrate a viable visual pathway that can operate in the absence of V1, in accordance with studies in human patients and lesion studies in monkeys^{1-8,11,12}.

We next investigated the components of the pathway that provide V1-bypassing input to the extrastriate cortex and support visual performance. Previous work has shown that direct anatomical projections exist from the LGN, the main thalamic relay between the retina and the primary visual cortex, to several extrastriate visual areas^{13,14}. We therefore proposed that residual activity in the extrastriate cortex, and corresponding behavioural performance, is the result of sensory signals transmitted directly from the LGN. To examine this possibility, we temporarily disrupted neural activity within the LGN of V1-lesioned monkeys by locally injecting the GABA_A-receptor agonist THIP¹⁵ (Methods Summary), and measured the effects on cortical fMRI responses and behavioural performance. Specifically, we reversibly inactivated the posterior part of the LGN, which represents the parafoveal

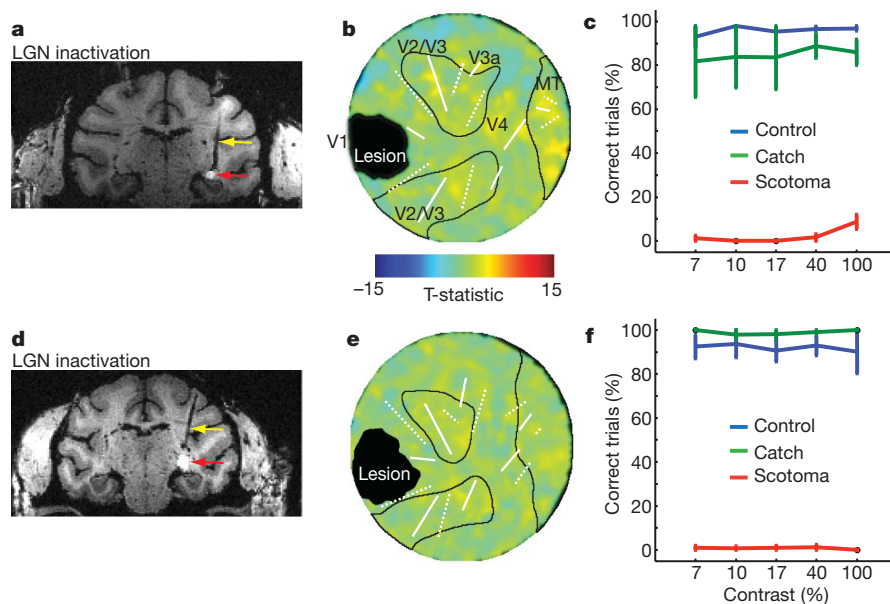


Figure 3 | Role of the LGN in driving V1-independent visual processing. **a**, We inactivated the LGN by injecting the GABA_A agonist THIP (Methods Summary). We co-injected the drug with the magnetic resonance contrast-agent gadolinium (total volume 2 μ l, Methods Summary), to visualize the site in magnetic resonance images. Here, a coronal section through the posterior part of monkey 1's LGN (+7 mm on the anterior-posterior axis in stereotactic coordinates) is shown. Injection of gadolinium resulted in a localized increase in the intensity of the T1-weighted magnetic resonance signal, with a diameter of \sim 3 mm (red arrow). We ensured that injections were reproducible across experiments by permanently implanting a magnetic-resonance-compatible cannula (yellow arrow). **b**, Functional activation map of macaque 1's left, lesioned, hemisphere to visual

stimulation inside the scotoma (35 stimulation cycles) during inactivation of the LGN. LGN inactivation results in the elimination of V1-independent visual responses (Fig. 2b). **c**, Monkey 1's performance in detecting visual targets at different luminance contrasts. Data represent mean \pm s.e.m. performance from three experiments with THIP injections into the LGN. The injections eliminated the monkey's ability to detect a target inside the scotoma. **d**, Inactivation of macaque 2's posterior LGN. **e**, Activation map of monkey 2's right, lesioned, hemisphere to visual stimulation inside the scotoma (60 stimulation cycles) during LGN inactivation. **f**, Monkey 2's performance for correctly detecting targets during LGN inactivation. Data represent the mean \pm s.e.m. performance in three experiments with THIP injections.

visual hemifield and covers the scotoma-affected region (Methods Summary), on multiple occasions via chronically implanted guide tubes compatible with magnetic resonance. The magnetic resonance contrast-agent gadolinium was co-injected along with THIP, allowing us to visualize the spread of the injection in the tissue. In both monkeys (Fig. 3a, d), the 2 μ l injection diffused to an effective diameter of approximately 3 mm in the caudal LGN, as visualized by the gadolinium (Fig. 3a, d).

After we had inactivated the LGN, virtually all extrastriate responses in the V1-lesioned hemispheres disappeared (Fig. 3b, e), indicating that the residual activation to stimuli presented in the scotoma had indeed reached the extrastriate cortex by means of direct projections from the LGN. Moreover, inactivation of the LGN abolished the animals' residual capacity to detect high-contrast stimuli presented to the scotoma region of the visual field (red line, Fig. 3c, f), demonstrating that the LGN is the critical thalamic link that supports behavioural performance in blindsight. As a control, detection of visual stimuli in the opposite hemifield (outside the scotoma) was unaffected.

To obtain a more quantitative assessment of the amount of information transmitted directly via the LGN, we compared the strength of fMRI responses under normal visual stimulation conditions to those obtained inside the scotoma, with and without additional LGN inactivation, across all experimental sessions (Fig. 4). On average, across all monkeys and extrastriate areas, scotoma stimulation with the LGN intact had fMRI activation of \sim 20% of that under normal conditions. This finding is in good qualitative agreement with previously reported fMRI activation patterns of human and monkey blindsight subjects^{6,7,11} and with single-unit recordings in area V5/MT of macaque monkeys with chronic V1 lesions¹². In addition, inactivating the LGN reduced activation levels to less than 5% of normal.

Apart from demonstrating the role of the LGN in supporting blindsight, these data reveal several interesting features of V1-independent

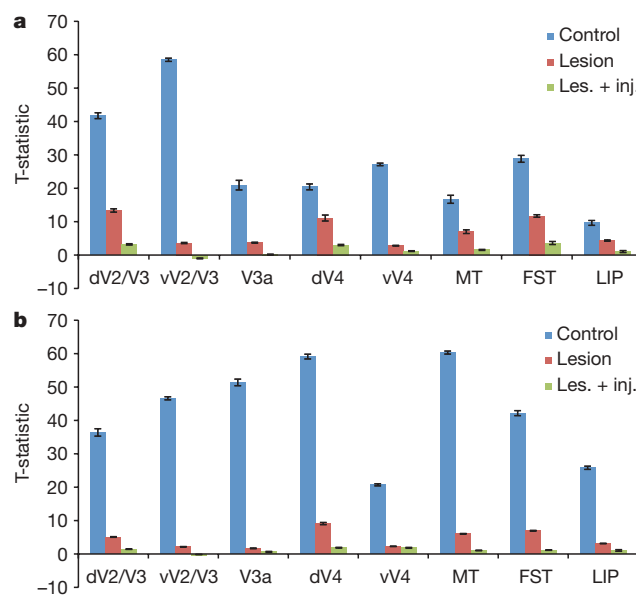


Figure 4 | Quantitative summary of mean fMRI activation levels. In extrastriate areas under normal conditions (V1 and LGN intact, blue bars); in the absence of V1 input (lesion, red bars); and in the absence of input from V1 and the LGN (Les. + inj., green bars). **a**, Data collected from monkey 1 and corresponding to the mean \pm s.e.m. *t*-statistic obtained during 85 visual stimulation cycles without LGN inactivation and 35 stimulation cycles with LGN inactivation. **b**, Data from experiments with monkey 2, in which the mean \pm s.e.m. *t*-statistic has been computed over 95 stimulation cycles without LGN inactivation and 60 stimulation cycles with LGN inactivation. On average across all areas and monkeys, fMRI activation in extrastriate areas is reduced by \sim 80% when V1 input is missing. Additional LGN inactivation reduces activity by more than 95% compared to normal levels.

vision. For example, the asymmetry of visual responses in areas V2 and V3 to stimuli in the scotoma, which has previously been observed in blindsight patient GY⁷, may reflect the differential contributions of parallel visual streams to upper- and lower-field vision: namely, that a larger proportion of neurons in the retina and the LGN respond to lower-visual-field stimulation than to upper-visual-field stimulation¹⁶. Psychophysical evidence suggests that this bias is primarily related to the magnocellular system¹⁷, which, at the level of the retina, is also the system that is less affected by retrograde degeneration following V1 injury¹⁸. Thus, one possibility for the observed asymmetry following striate cortex lesions is that the normal visual-field asymmetry of the magnocellular system is unmasked by post-lesional neurodegeneration.

The near-complete drop in both extrastriate activation and behavioural performance not only implicates the LGN as a critical hub for blindsight, but also argues against the existence of pathways that do not involve the LGN. Blindsight functions have been observed for decades in a number of different species, and have traditionally been attributed to a second visual pathway in which retinal information is relayed via the superior colliculus and a secondary thalamic nucleus, the pulvinar, to the extrastriate cortex¹⁹. Although the role of the superior colliculus in mediating blindsight functions and V1-independent responses in area V5/MT has been demonstrated^{20,21}, there is presently no direct evidence that the pulvinar is involved. On the contrary, the pulvinar may have minimal contribution for the following reasons: its anatomical basis as a first-order visual-relay is in question²² (however, see refs 23 and 24); its neural responses appear to be driven more by cortical than by collicular inputs²⁵; there is no residual vision following LGN lesions²⁶; and neural activity in area V5/MT is eliminated during LGN inactivation²⁷.

Conversely, contribution of the LGN to blindsight has sometimes been left as an open possibility^{4,21}, particularly since the neural degeneration following V1 ablation selectively spares LGN cells that project directly to the extrastriate cortex²⁸. These V1-bypassing projection neurons appear to belong chiefly to the koniocellular system, whose neurons reside primarily in the intercalated LGN layers^{13,14,22}. Interestingly, it is these koniocellular-rich layers that receive input from the superior colliculus^{22,29}. This may explain the previously described effects of superior colliculus ablation on V1-independent visual processing^{20,21}. Finally, recent observations using diffusion-tensor magnetic resonance imaging in a human blindsight patient many years after a V1 lesion show significant projections between the LGN and area V5/MT³⁰, although the direction of the projection could not be established.

Our data demonstrate that the LGN has a causal role in V1-independent visual function. We propose that this residual function is mediated by neurons in the intercalated layers of the LGN, whose direct projections to the extrastriate cortex may not only support residual vision following V1 lesions, but may also serve as a shortcut to the high-level cortex during normal vision. In providing short-latency, eye-specific signals to high-level visual cortex, such a shortcut could serve to facilitate some forms of rapid behavioural responses to visual stimuli.

METHODS SUMMARY

The main experiments were carried out in two healthy adult monkeys (*Macaca mulatta*): one male (8 kg weight; monkey 1) and one female (5 kg weight; monkey 2). Additional control experiments were conducted in a third healthy adult monkey (female, 5 kg weight). All procedures followed the Institute of Laboratory Animal Research (part of the National Research Council of the National Academy of Sciences) guidelines and were approved by the National Institute of Mental Health (NIMH) Animal Care and Use Committee. To immobilize the head during experiments and to record eye movements during behavioural testing, we implanted headposts and eye coils following standard procedures. We caused V1-area lesions by coagulating pial vessels over the intended lesion area on the V1 operculum, and by aspirating grey matter within this area. In both monkeys the lesions were located ~2–7° visual eccentricities away from the fovea (monkeys had no problems maintaining fixation), covering

between one-third and one-half of opercular V1. We used a lesion in a third monkey, covering all of opercular V1 and large parts of the adjacent V2 (Supplementary Fig. 6), to evaluate the possibility of scattered-light effects on intact grey-matter tissue in the first two, smaller lesioned, monkeys. To reach the LGN for inactivation, we chronically implanted magnetic-resonance-compatible fused-silica guide tubes (Plastics One) in monkeys 1 and 2, using a frameless stereotaxy procedure (Brainsight, Rogue Research). For the experiments, we injected the GABA_A agonist THIP (Tocris; concentration: 6.67 μg μl⁻¹, dissolved in sterile saline, pH 7.4; volume: 2 μl; rate: 0.5–1 μl min⁻¹) for LGN inactivation together with the magnetic resonance contrast-agent gadolinium (Berlex Imaging, 5 mM) to visualize the site and extent of the injection in a magnetic resonance image.

Received 1 December 2009; accepted 18 May 2010.

Published online 23 June 2010.

- Weiskrantz, L., Warrington, E. K. & Sanders, M. D. Visual capacity in the hemianopic field following a restricted occipital ablation. *Brain* **97**, 709–728 (1974).
- Cowey, A. & Stoerig, P. Blindsight in monkeys. *Nature* **373**, 247–249 (1995).
- Keating, E. G. Residual spatial vision in the monkey after removal of striate and precipital cortex. *Brain Res.* **187**, 271–290 (1980).
- Cowey, A. The blindsight saga. *Exp. Brain Res.* **200**, 3–24 (2010).
- Brewer, A. A., Press, W. A., Logothetis, N. K. & Wandell, B. A. Visual areas in macaque cortex measured using functional magnetic resonance imaging. *J. Neurosci.* **22**, 10416–10426 (2002).
- Schmid, M. C., Panagiotaropoulos, T., Augath, M. A., Logothetis, N. K. & Smirnakis, S. M. Visually driven activation in macaque areas V2 and V3 without input from the primary visual cortex. *PLoS ONE* **4**, e5527, doi:10.1371/journal.pone.0005527 (2009).
- Baseler, H. A., Morland, A. B. & Wandell, B. A. Topographic organization of human visual areas in the absence of input from primary cortex. *J. Neurosci.* **19**, 2619–2627 (1999).
- Cowey, A. & Stoerig, P. Visual detection in monkeys with blindsight. *Neuropsychologia* **35**, 929–939 (1997).
- Collins, C. E., Lyon, D. C. & Kaas, J. H. Responses of neurons in the middle temporal visual area after long-standing lesions of the primary visual cortex in adult new world monkeys. *J. Neurosci.* **23**, 2251–2264 (2003).
- Campion, J., Latto, R. & Smith, Y. M. Is blindsight an effect of scattered light, spared cortex, and near-threshold vision? *Behav. Brain Sci.* **6**, 423–447 (1983).
- Goebel, R., Muckli, L., Zanella, F. E., Singer, W. & Stoerig, P. Sustained extrastriate cortical activation without visual awareness revealed by fMRI studies of hemianopic patients. *Vision Res.* **41**, 1459–1474 (2001).
- Rodman, H. R., Gross, C. G. & Albright, T. D. Afferent basis of visual response properties in area MT of the macaque. I. Effects of striate cortex removal. *J. Neurosci.* **9**, 2033–2050 (1989).
- Sincich, L. C., Park, K. F., Wohlgenuth, M. J. & Horton, J. C. Bypassing V1: a direct geniculate input to area MT. *Nature Neurosci.* **7**, 1123–1128 (2004).
- Bullier, J. & Kennedy, H. Projection of the lateral geniculate nucleus onto cortical area V2 in the macaque monkey. *Exp. Brain Res.* **53**, 168–172 (1983).
- Cope, D. W., Hughes, S. W. & Crunelli, V. GABA_A receptor-mediated tonic inhibition in thalamic neurons. *J. Neurosci.* **25**, 11553–11563 (2005).
- Curcio, C. A. & Allen, K. A. Topography of ganglion cells in human retina. *J. Comp. Neurol.* **300**, 5–25 (1990).
- McAnany, J. J. & Levine, M. W. Magnocellular and parvocellular visual pathway contributions to visual field anisotropies. *Vision Res.* **47**, 2327–2336 (2007).
- Cowey, A., Stoerig, P. & Perry, V. H. Transneuronal retrograde degeneration of retinal ganglion cells after damage to striate cortex in macaque monkeys: selective loss of Pβ cells. *Neuroscience* **29**, 65–80 (1989).
- Diamond, I. T. & Hall, W. C. Evolution of neocortex. *Science* **164**, 251–262 (1969).
- Mohler, C. W. & Wurtz, R. H. Role of striate cortex and superior colliculus in visual guidance of saccadic eye movements in monkeys. *J. Neurophysiol.* **40**, 74–94 (1977).
- Rodman, H. R., Gross, C. G. & Albright, T. D. Afferent basis of visual response properties in area MT of the macaque. II. Effects of superior colliculus removal. *J. Neurosci.* **10**, 1154–1164 (1990).
- Stepniewska, I., Qi, H. X. & Kaas, J. H. Do superior colliculus projection zones in the inferior pulvinar project to MT in primates? *Eur. J. Neurosci.* **11**, 469–480 (1999).
- Berman, R. A. & Wurtz, R. H. Functional identification of a pulvinar path from superior colliculus to cortical area MT. *J. Neurosci.* **30**, 6342–6354 (2010).
- Lyon, D. C., Nassi, J. J. & Callaway, E. M. A dysynaptic relay from superior colliculus to dorsal stream visual cortex in macaque monkey. *Neuron* **65**, 270–279 (2010).
- Bender, D. B. Visual activation of neurons in the primate pulvinar depends on cortex but not colliculus. *Brain Res.* **279**, 258–261 (1983).
- Schiller, P. H., Logothetis, N. K. & Charles, E. R. Functions of the colour-opponent and broad-band channels of the visual system. *Nature* **343**, 68–70 (1990).
- Maunsell, J. H., Nealey, T. A. & DePriest, D. D. Magnocellular and parvocellular contributions to responses in the middle temporal visual area (MT) of the macaque monkey. *J. Neurosci.* **10**, 3323–3334 (1990).
- Cowey, A. & Stoerig, P. Projection patterns of surviving neurons in the dorsal lateral geniculate nucleus following discrete lesions of striate cortex: implications for residual vision. *Exp. Brain Res.* **75**, 631–638 (1989).

29. Harting, J. K., Huerta, M. F., Hashikawa, T. & van Lieshout, D. P. Projection of the mammalian superior colliculus upon the dorsal lateral geniculate nucleus: organization of tectogeniculate pathways in nineteen species. *J. Comp. Neurol.* **304**, 275–306 (1991).
30. Bridge, H., Thomas, O., Jbabdi, S. & Cowey, A. Changes in connectivity after visual cortical brain damage underlie altered visual function. *Brain* **131**, 1433–1444 (2008).

Supplementary Information is linked to the online version of the paper at www.nature.com/nature.

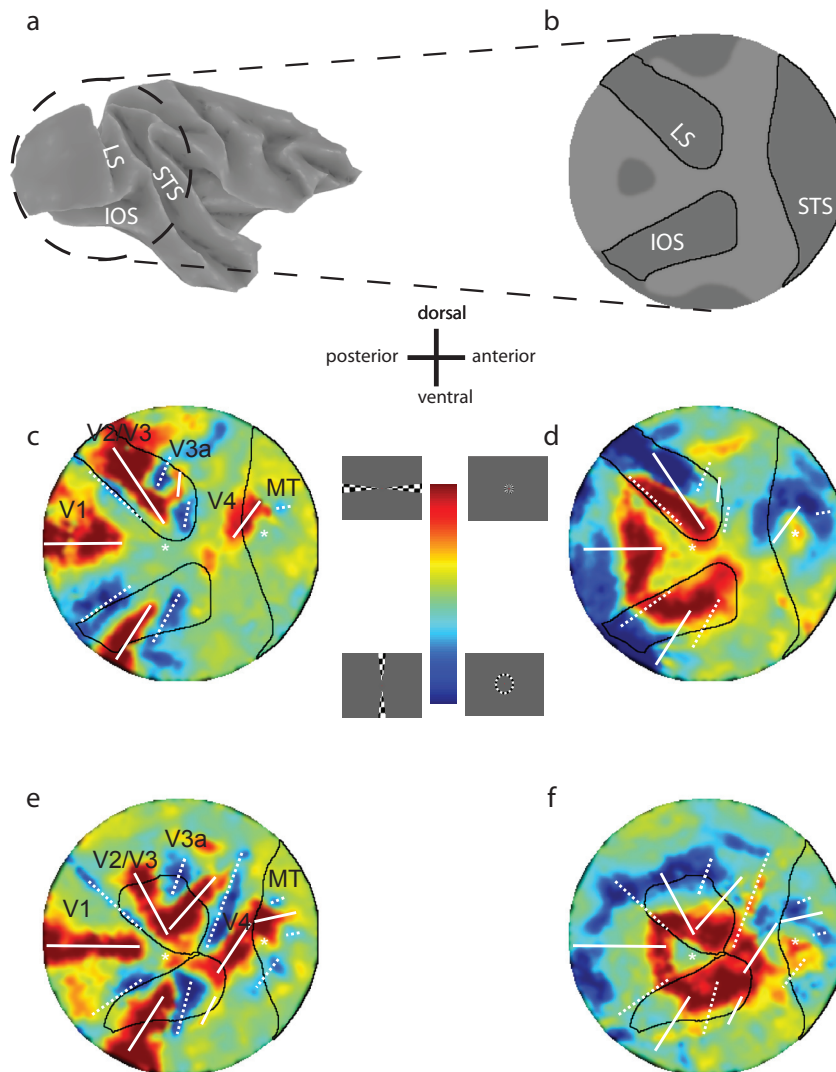
Acknowledgements We thank A. Maier and D. McMahon for comments on the manuscript; S. Smirnakis, R. Berman, R. Wurtz, B. Richmond, S. Guderian and M. Fukushima for discussions; C. Zhu and H. Merkle for magnetic resonance coil construction; K. Smith, N. Phipps, J. Yu, G. Dold, D. Ide and T. Talbot for technical assistance; D. Sheinberg for developing visual stimulation software; and members of the Brian Wandell laboratory for developing and sharing mrVista software. This

work was supported by the Intramural Research Programme of the NIMH, the NINDS, and the NEI.

Author Contributions M.C.S. took the primary lead for all aspects of this work and wrote the paper; S.W.M. helped with experiments and analysis; J.T. helped with the experiments and developed the inactivation method; R.C.S. created the lesions; M.W. developed the inactivation method; A.J.P. helped with experiments and analysis; F.Q.Y. developed pre-processing software and optimized magnetic resonance sequences; and D.A.L. provided resources, acted in a supervisory role on all aspects of this work and wrote the paper.

Author Information Reprints and permissions information is available at www.nature.com/reprints. The authors declare no competing financial interests. Readers are welcome to comment on the online version of this article at www.nature.com/nature. Correspondence and requests for materials should be addressed to M.C.S. (schmidmicha@gmail.com)

SUPPLEMENTARY INFORMATION

**Supplementary Figure 1.** Retinotopic mapping of the non-lesioned hemisphere. **a.**

Inflated 3D representation of monkey 1's non-lesioned hemisphere seen from the side.

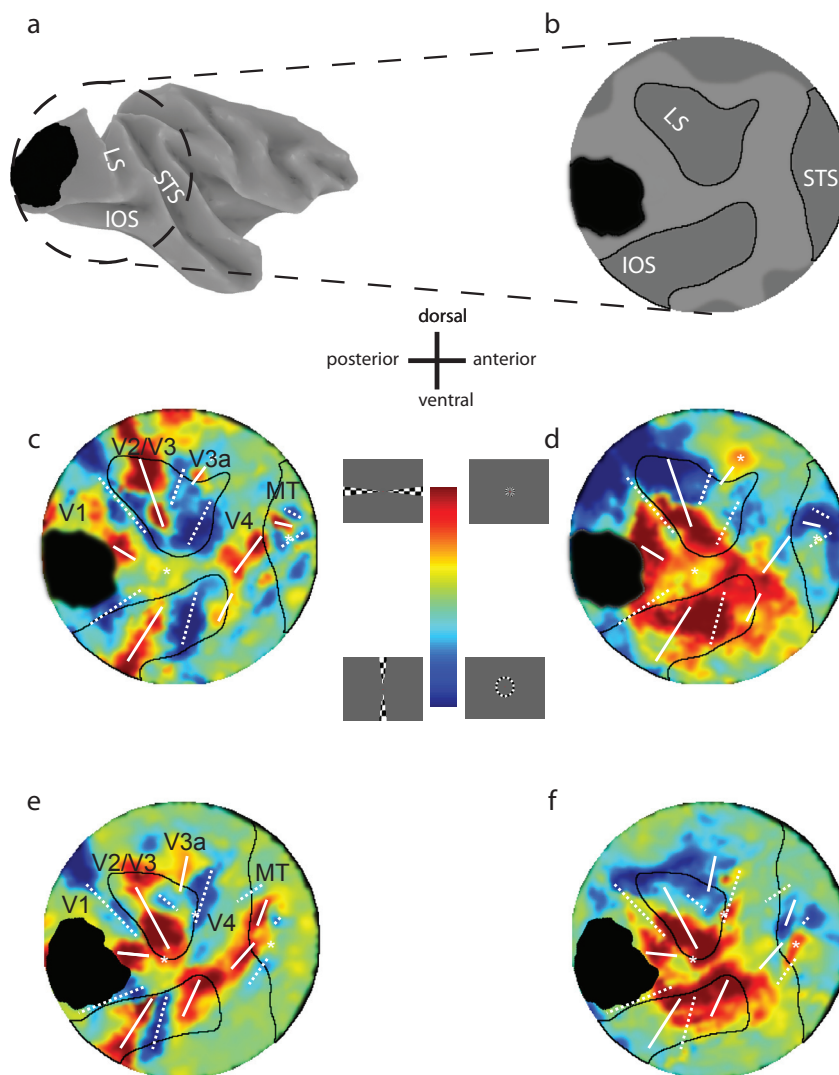
b. Flat map of monkey 1's non-lesioned hemisphere. **c.** Functional activation map of

monkey 1's non-lesioned hemisphere during mapping with meridian stimuli. Horizontal meridian representations are highlighted as solid lines, vertical meridian representations are marked with dotted lines. The alternation pattern between these visual field

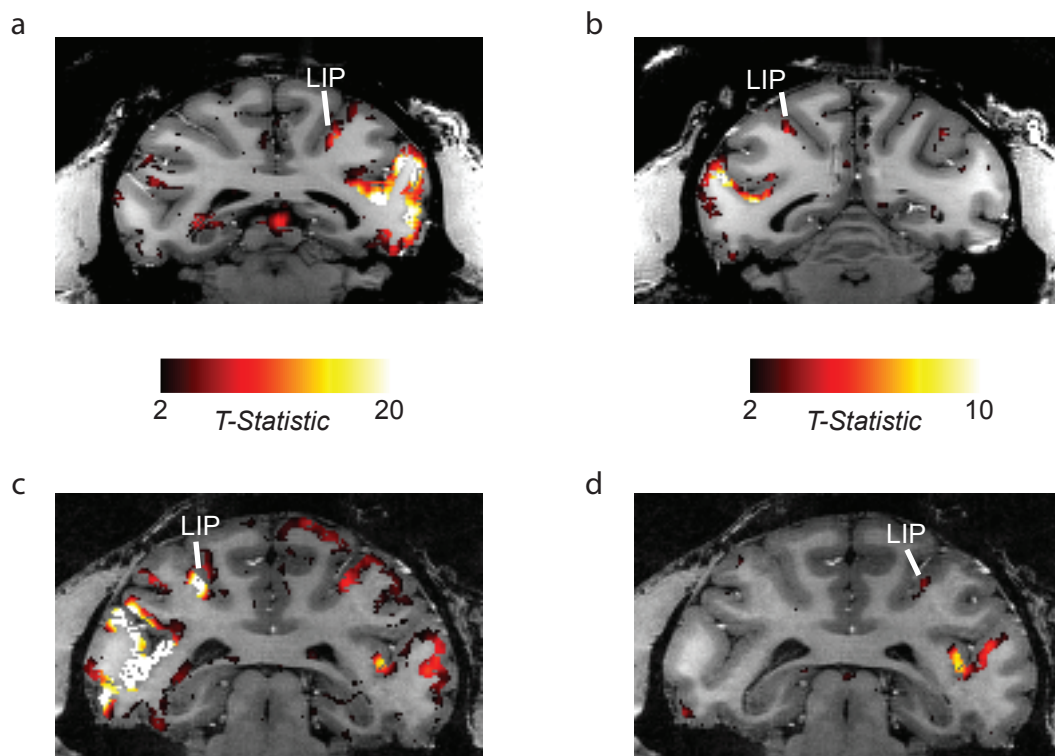
representations provides the basis for identifying and isolating visual areas for further quantitative analysis. **d.** Functional activation map of monkey 1's non-lesioned

hemisphere during mapping with annuli presented at either one of three possible positions (2°, 4° and 7°). The contrast displayed here corresponds to the difference between 2° and 7° stimulus position conditions. The foveal representation is indicated

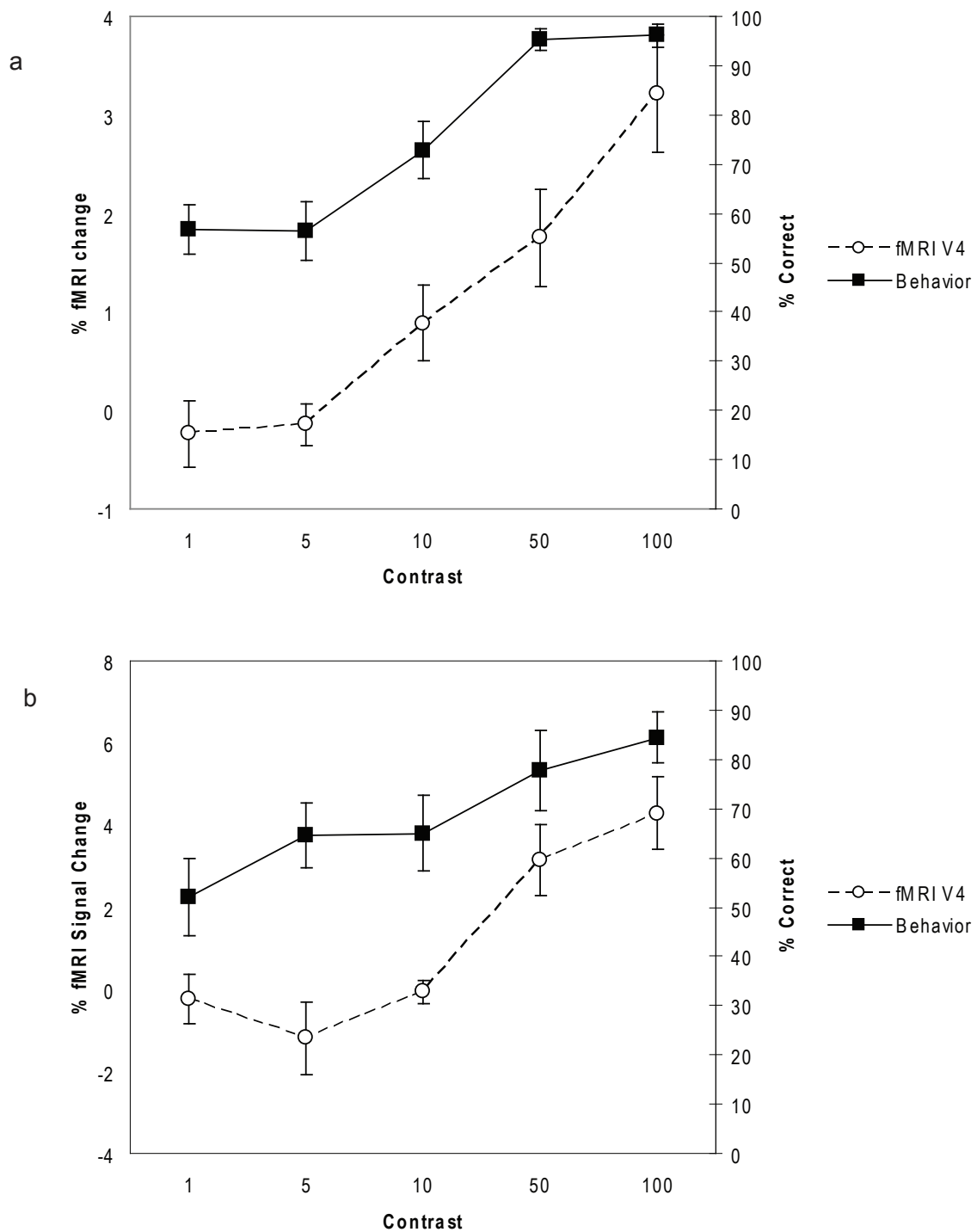
with an asterisk. **e.** Functional activation in monkey 2's non-lesioned hemisphere during meridian mapping. **f.** Ring retinotopy in monkey 2's non-lesioned hemisphere.



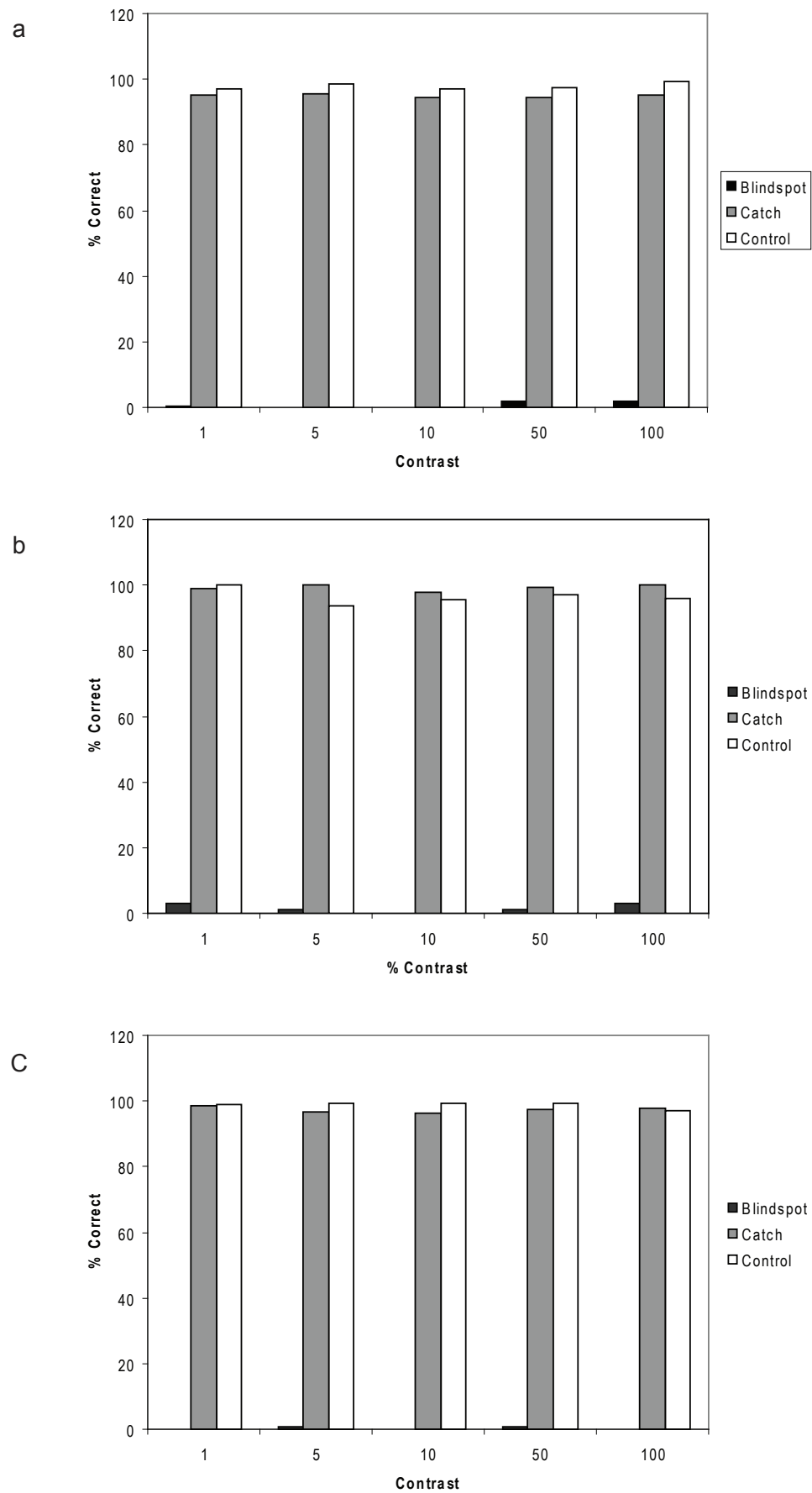
Supplementary Figure 2. Retinotopic mapping of the lesioned hemisphere. **a.** Inflated 3D representation of monkey 1's lesioned hemisphere seen from the side. **b.** Flat map of monkey 1's lesioned hemisphere. **c.** Functional activation map of monkey 1's lesioned hemisphere during mapping with meridian stimuli. Horizontal meridian representations are highlighted as solid lines, vertical meridian representations are marked with dotted lines. The alternation pattern between these visual field representations provides the basis for identifying and isolating visual areas for further quantitative analysis. **d.** Functional activation map of monkey 1's lesioned hemisphere during mapping with stimuli annuli presented at either one of three possible positions (2° , 4° and 7°). The contrast displayed here corresponds to the difference between 2° and 7° stimulus position conditions. **e.** Functional activation in monkey 2's lesioned hemisphere during meridian mapping. **f.** Ring retinotopy of monkey 2's lesioned hemisphere.



Supplementary Figure 3. Visually driven responses in parietal area LIP. **a.** Coronal slice of macaque 1's brain at the level of the intraparietal sulcus. The stimulus was a 2° diameter rotating checkerboard placed at 4° eccentricity in the left visual field outside the scotoma (methods summary). Visual activation to 85 stimulation cycles is thresholded (t -statistic >2), color-coded and overlaid onto the anatomy. The stimulus effectively drives responses in extrastriate cortex and parietal area LIP. **b.** Functional activation in monkey 1 to visual stimulation in the scotoma (right visual field). In the absence of V1 input, extrastriate areas and parietal area LIP continue to be visually responsive. **c.** Functional activation in monkey 2's occipital and parietal lobes to visual stimulation outside the scotoma (left visual field, 95 stimulation cycles). **d.** Functional activation in monkey 2 to visual stimulation in the scotoma (left visual field, 95 visual stimulation cycles) revealing a similar V1-independent activation pattern in visual and parietal areas as in monkey 1 (panel b).

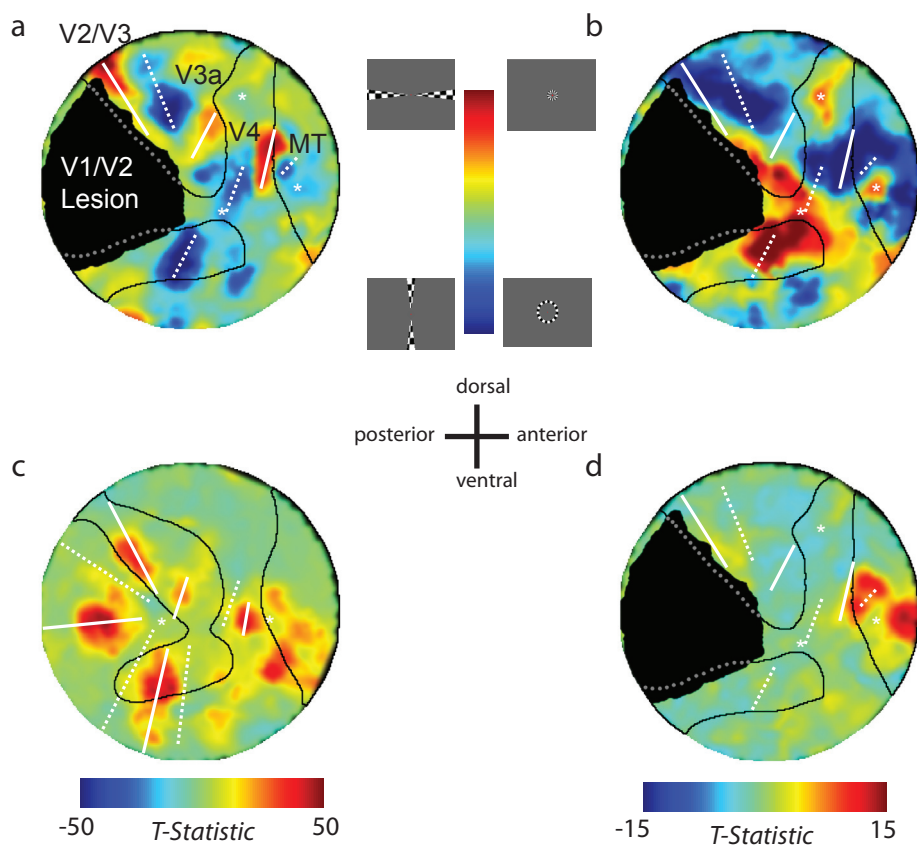


Supplementary Figure 4. Direct comparison between V1-independent behaviour and fMRI responses using the same visual stimulus. **a.** Monkey 3's (large V1/V2 lesion) behavioural and fMRI responses to a 2° diameter rotating checkerboard stimulus presented inside the scotoma as a function of the stimulus luminance contrast (supplementary methods). FMRI responses were derived from area V4. Note the tight correlation between fMRI and behavioural responses. **b.** FMRI and behavioural responses of monkey 1 to visual stimulation restricted to the scotoma. Increasing the stimulus contrast results in an increase in both behavioural and fMRI responses.



Supplementary Figure 5. Behavioural performance to visual stimulation in the blindspot region. The same 2° rotating stimulus used in the main experiments was

presented monocularly in the blindspot region (center at 16° eccentricity) of monkeys 1 (panel a, 3000 trials), 2 (panel b, 1500 trials), and 3 (panel c, 2000 trials) as a function of luminance contrast (supplementary figure 4). In none of the monkeys did the performance to detect the stimulus presented in the blindspot area reach the 5% correct level. In contrast, monkeys had no problem in detecting visual stimuli presented at 16° contralateral to the blindspot region or to remain fixating during catch trials. The monkey's ability to correctly detect visual stimuli presented in the blindspot area was significantly compromised compared to their ability to detect the identical stimuli when presented in the scotoma (supplementary figure 4). As the size of the scotoma and blindspot regions closely match each other, it is very unlikely that scattering light stimulating intact V1 tissue surrounding the lesion can account for the behavioural performance in the scotoma.



Supplementary Figure 6. Extrastriate activation after a V1/V2 lesion. **a.** Meridional mapping of monkey 3's lesioned hemisphere. Horizontal meridian representations are highlighted as white solid lines, vertical meridian representations are marked with white dotted lines. The area covered by the V1/V2 lesion is shown in black. Black solid lines highlight the sulcal pattern. A gray dotted line shows the part of the sulcus affected by the lesion. **b.** Ring retinotopy of monkey 3's lesioned hemisphere (supplementary figure 2 d,f). **c.** Functional activation in monkey 3's non-lesioned hemisphere to stimulation with a 2° diameter rotating checkerboard stimulus (figure 2 a, d). **d.** Functional activation in the lesioned hemisphere of monkey 3 to stimulation with a 2° rotating checkerboard in the scotoma (figure 2 b, e). Note the presence of visually driven responses in areas V4, V5/MT, FST despite the absence of direct V1/V2 input. Activation as seen in figure 2 b,e for monkeys with smaller lesions can therefore not be attributed to the effects of scattering light on intact V1 gray matter surrounding the lesion.

Supplementary methods

MRI procedures. MR experiments were conducted in a vertical 4.7 T scanner with a 60 cm diameter bore (Biospec, Bruker Medical, Ettlingen, Germany). The system was equipped with a 60 mT/m (0.15 ms rise time) actively shielded gradient coil (Biospec, Bruker Medical, Ettlingen, Germany). A radiofrequency coil (Monkey 1: 8-channel transmit/receive coil (Rapid) with a 140 mm transmit diameter, 113 mm receive diameter; Monkey 2: custom-made single channel coil, with 100 mm inner diameter) was placed over the monkey's occipital lobe to acquire images from the visual cortex. To optimize homogeneity of the MR signal from visual cortex, fieldmap-based shimming of this area was performed using a $62 \times 42 \times 42 \text{ mm}^3$ box for Monkey 1 and $56 \times 42.25 \times 26.25 \text{ mm}^3$ box for Monkey 2. Functional imaging sessions were preceded by the intravenous injection of monocrySTALLINE iron oxide nanoparticles (MION), a ferromagnetic contrast agent that provides higher contrast to noise than the intrinsic BOLD signal, and provides a measure of changes in regional cerebral blood volume^{1,2}. Acquisition of functional data was performed using single-shot gradient-recalled EPI with a voxel resolution of $1.5 \times 1.5 \times 2 \text{ mm}^3$ (16 slices, FOV = 90 mm x 45 mm, Matrix = 72 x 36, TR = 2000 ms, TE = 14.6 ms, FA = 75 deg). A sequence of 150 images was acquired during a single functional scan. Structural MR images of the visual cortex ($0.5 \times 0.5 \times 2 \text{ mm}^3$ resolution) were obtained within each experimental session using the 3D-Mdeft sequence³ and served to overlay functional activation maps with the underlying anatomy. In addition, high-resolution 3D-Mdeft images³ ($0.5 \times 0.5 \times 0.5 \text{ mm}^3$ resolution) with global brain coverage were acquired in separate sessions 1) to coregister functional data across experiments, and 2) to segment gray and white matter and create flat maps of visual cortex.

Behavioural testing. Behavioural testing was conducted outside the MR environment in a noise-shielded booth. Visual stimuli were created using custom made software and

presented on a TFT screen (Samsung) at a resolution of 1280 x 1024. The behaviour of the monkey was controlled using custom-made software based on the real-time operating system QNX. Eye movements were assessed using the scleral search coil technique⁴. To assess the animal's visual sensitivity inside the scotoma area and compare it to identical conditions in the normal visual field the following experimental setup was used: A central fixation spot (0.2° radius) appeared for 1 second during which the monkey had to acquire fixation within 0.8° radius around the spot. Subsequently, a target spot (0.2° radius) appeared in one of three target positions: 1) inside the scotoma at 4° eccentricity (monkey 1: 1° in the upper visual field, monkey 2: at the horizontal meridian), 2) at the eccentricity-matched position in the non-lesioned hemifield ("control"), 3) at the initial fixation position ("catch trial"). The position of the stimulus varied randomly from trial to trial. Upon leaving the initial fixation window, the monkey was given 250 ms to execute a saccade towards the target. A trial was terminated when the monkey's saccade endpoint was within 1° radius from the target for at least 1 second. The animals received a drop of juice for every correct detection trial. To assess the monkey's sensitivity to detect the target we systematically varied the luminance of the target with respect to the background. The luminance of the background was 2.5 cd/m². We varied the luminance of the target spot with respect to the background to yield 5 different contrast levels.

Visual stimulation and behavioural paradigm during fMRI sessions. All experiments were conducted while the animal was awake and performing a passive fixation task throughout the duration of a scan while visual stimuli were periodically displayed in the periphery. Stimuli were presented using a projector (Silent Vision, Avotec Inc.) at its native resolution of 1280 x 1024. Stimuli were presented through a backlit projection screen, visible to the subject by a mirror mounted on the primate chair. Eye movements were recorded using an infrared sensitive camera (MRC Systems GmbH) and an eye tracking system (SensoMotoric Instruments). The monkey was

required to maintain fixation within 2° radius of a centrally presented fixation spot (0.4° radius) throughout the scan only allowing time for occasional blinks. To motivate the monkey for maintaining fixation for these long time periods (5 minutes), he was rewarded with a drop of juice every 2 seconds and the amount of juice increased with increasing fixation duration. Aborts (e.g. due to saccades) resulted in a delay for reward and a resetting of the juice amount to baseline levels. The procedure proved highly effective as monkeys rarely aborted a trial. For the analysis we only included scans in which the monkey maintained fixation for more than 95% of the time.

Our basic paradigm to obtain statistical maps of cortical activation consisted of blocks in which a rotating checkerboard pattern (~ 3.5 Hz visual modulation at 100% contrast) reversed its direction of rotation every 1.5 seconds and alternated with periods in which no stimulus was present on the gray background (mean luminance: 12 cd/deg). Stimulation and blank periods had a duration of 30 seconds; 5 stimulation cycles were shown during a single MR scan. To delineate the boundaries between visual areas, we used checkerboard patterns with the shape of an annulus (eccentricity mapping: 3 annuli at 1° , 4° and 7° , each with a width of 1°) and wedge shaped versions of the stimulus centered over the horizontal versus vertical meridians of the visual field (12° wedge angle, extending from 1° to 25°). To assess the strength of activation in extrastriate areas in the absence of V1 input or in the absence of V1 and geniculate input, we used a version of the rotating checkerboard stimulus that was restricted to the behaviourally determined scotoma of the stimulus. For monkey 1 the stimulus was centered 1° above the horizontal meridian, 4° from the midline in the right visual field. For monkey 2 the stimulus was centered on the horizontal meridian, 4° from the midline in the left visual field. For both monkeys, the stimulus had a radius of 2° .

Data analysis. Both behavioural and fMRI data sets were analyzed in MATLAB (MathWorks). FMRI data were preprocessed using the PLACE method to correct for

image distortions due to local inhomogeneities⁵ and the AFNI 3Dwarp function⁶ to correct for the effects of translational motions in the images. Single images that were grossly distorted due to motion (intensity of 6 STD > mean of all images in a ROI outside the brain) were removed from further analysis. Using this criterion, up to 2 images were removed in a typical experiment. Statistical analysis, co-registration of data across sessions, gray/white matter segmentation, and construction of cortical flat maps were performed using the mrVista software (<http://white.stanford.edu/software>). In brief, the GLM was computed between the time course of individual voxels and a predictor variable that was created by convolving the design matrix of the stimulation sequence with a hemodynamic response function. Activation maps displayed in the figures represent the t-statistic between visual stimulation and baseline.

- 1 Vanduffel, W. *et al.* Visual motion processing investigated using contrast agent-enhanced fMRI in awake behaving monkeys. *Neuron* **32**, 565-577 (2001).
- 2 Smirnakis, S. M. *et al.* Spatial specificity of BOLD versus cerebral blood volume fMRI for mapping cortical organization. *J Cereb Blood Flow Metab* (2007).
- 3 Lee, J. H. *et al.* High contrast and fast three-dimensional magnetic resonance imaging at high fields. *Magnetic Resonance in Medicine* **34**, 308 (1995).
- 4 Judge, S. J., Richmond, B. J. & Chu, F. C. Implantation of magnetic search coils for measurement of eye position: an improved method. *Vision Res* **20**, 535-538, doi:0042-6989(80)90128-5 [pii] (1980).
- 5 Xiang, Q. S. & Ye, F. Q. Correction for geometric distortion and N/2 ghosting in EPI by phase labeling for additional coordinate encoding (PLACE). *Magn Reson Med* **57**, 731-741, doi:10.1002/mrm.21187 (2007).
- 6 Cox, R. W. AFNI: software for analysis and visualization of functional magnetic resonance neuroimages. *Comput Biomed Res* **29**, 162-173, doi:S0010480996900142 [pii] (1996).